PAPER

Chronic neural interfacing with cerebral cortex using single-walled carbon nanotube-polymer grids

Journal of Neural Engineering

PAPER

Chronic neural interfacing with cerebral cortex using single-walled carbon nanotube-polymer grids

Luigi Pavone[1,2,8,9], **Slavianka Moyanova**[2,8], **Federica Mastroiacovo**[2], **Laura Fazi**[3,4], **Carla Busceti**[2], **Anderson Gaglione**[2], **Katiuscia Martinello**[2], **Sergio Fucile**[2,5], **Domenico Bucci**[2], **Anna Prioriello**[2], **Ferdinando Nicoletti**[2,5], **Francesco Fornai**[2,6], **Piero Morales**[3,7] and **Roberto Senesi**[3,4]

[1] Department of Life and Health 'V. Tiberio', University of Molise, Campobasso, Italy
[2] IRCCS Neuromed, Via Atinense 18, 86077, Pozzilli (IS), Italy
[3] NAST Center, University of Rome 'Tor Vergata', Rome 00133, Italy
[4] Physics Department, University of Rome 'Tor Vergata', Rome 00133, Italy
[5] Department of Physiology and Pharmacology, University of Rome 'La Sapienza', Rome 00161, Italy
[6] Department of Translational Research and New Technologies in Medicine and Surgery, University of Pisa, Via Roma 55, 56126, Pisa, Italy
[7] SONS School of Neutron Scattering 'F.P. Ricci', Rome 00133, Italy
[8] These authors contributed equally
[9] Author to whom any correspondence should be addressed.

E-mail: bioingegneria@neuromed.it

RECEIVED
14 October 2019

REVISED
27 May 2020

ACCEPTED FOR PUBLICATION
2 June 2020

PUBLISHED
2 July 2020

Keywords: single-walled carbon nanotube, brain machine interface, subdural ECoG arrays, polymer carbon nanotubes composite, ECoG, biocompatibility, neural interfaces

Supplementary material for this article is available online

Abstract

Objective. The development of electrode arrays able to reliably record brain electrical activity is a critical issue in brain machine interface (BMI) technology. In the present study we undertook a comprehensive physico-chemical, physiological, histological and immunohistochemical characterization of new single-walled carbon nanotubes (SWCNT)-based electrode arrays grafted onto medium-density polyethylene (MD-PE) films. *Approach.* The long-term electrical stability, flexibility, and biocompatibility of the SWCNT arrays were investigated *in vivo* in laboratory rats by two-months recording and analysis of subdural electrocorticogram (ECoG). Ex-vivo characterization of a thin flexible and single probe SWCNT/polymer electrode is also provided. *Main results.* The SWCNT arrays were able to capture high quality and very stable ECoG signals across 8 weeks. The histological and immunohistochemical analyses demonstrated that SWCNT arrays show promising biocompatibility properties and may be used in chronic conditions. The SWCNT-based arrays are flexible and stretchable, providing low electrode-tissue impedance, and, therefore, high compliance with the irregular topography of the cortical surface. Finally, reliable evoked synaptic local field potentials in rat brain slices were recorded using a special SWCNT-polymer-based flexible electrode. *Significance.* The results demonstrate that the SWCNT arrays grafted in MD-PE are suitable for manufacturing flexible devices for subdural ECoG recording and might represent promising candidates for long-term neural implants for epilepsy monitoring or neuroprosthetic BMI.

1. Introduction

The electrocorticogram (ECoG) has been accepted as a good bioelectrical signal source for brain machine interface (BMI) applications [1–3]. The design and fabrication of array of electrodes for epidural or subdural ECoG recording, as a chronically implantable part of BMIs, should meet specific requirements [4–6]. In particular, the electrodes of these arrays should have stable electrical properties, including low electrode/cortical tissue impedance, good signal-to-noise ratio (SNR), appropriate mechanical properties and biocompatibility, especially for long-term use. Normally, the electrodes used for invasive subdural ECoG recordings in humans are metal disks tailored in grids embedded in a

plastic film (generally silicon rubber). Among others, platinum (Pt) is the most commonly used material for the fabrication of electrodes to record bioelectrical activity and stimulate brain structures, both in experimental animals and humans [6, 7]. However, commercially available subdural electrodes are not suitable for prolonged chronic applications, because they are rigid and heavy, causing inflammatory response [8, 9] and degradation of characteristics over time [10]. Significant research was carried out recently to improve the classical neural interfaces and reduce the tissue reaction [11–13]. For animal studies, grids incorporating metal electrodes such as gold [14] or titanium nitrite contacts [15] have been used for epidural ECoG recordings. There are also a few studies with subdural grids implanted on animals, based on platinum electrodes in silicone rubber [7] or poly 3,4-ethylenedioxythiophene [16]. New technology of interfaces fabrication using non-metal-based materials like carbon nanotubes (CNTs) is in progress [17–20]. Being biocompatible, stretchable, flexible, mechanically strong, and highly conducting, CNTs with their micrometric diameters have attracted great interest as a material in the clinically used ECoG arrays for neurobiological applications [21], as these properties are very important for bioelectrical activity recording and stimulation [22–25]. It should be remarked that bundled CNT represents in principle the ideal material for biomedical application because of its dual structure: it is indeed the strongest fully inert material with a nanometric elementary structure, while having a coiled and bundled superstructure in the micrometric range. It is therefore the least prone to releasing toxic nano-particles (because of its strength) and to producing hazardous interactions at the molecular level (because the micro-sized bundles do not allow penetration into cells or nanoenvironments of living organisms). At the same time, its inherently elastic structure minimizes damage to the surrounding tissue. No recordings with CNT-based ECoG arrays have yet been performed in humans and only few studies have examined the functionality of CNT grids implanted on animal's brain [17–19]. Single-walled carbon nanotubes (SWCNT), in particular, being much more thin and flexible than multi-walled carbon nanotubes (MWCNT), are at the forefront of novel nanoscale investigations due to their unique structure-dependent electronic and mechanical properties [26, 27]. To our knowledge, there are no reports of SWCNT-based devices tested for neuronal recording or stimulation neither *in-vivo*, nor *ex-vivo* or *in-vitro*. Very important features for ECoG electrode arrays are their flexibility and stretchability [28], properties that are intrinsic to the intertwined bundles structure of as-grown SWCNT. Furthermore, we recently showed that grafting SWCNT bundles on medium density-polyethylene (MD-PE) provide conductive tracks having reliable elasto-plastic properties [29]. We demonstrated in the same study that the SWCNT/MD-PE arrays were able to capture reliable and stable subdural ECoG in rats for 3 months, but we did not assess the flexibility of such arrays and their conformation to three-dimensional surfaces. The flexibility of ECoG electrode arrays can add perspectives for ECoG recordings from the human gyrencephalic brain that has many gyri and sulci. In fact, numerous cortical areas in humans involved in auditory, motor, visual and somatosensory processing are situated in sulci [30] are important targets for BMI applications. However, they are not easily reachable by the classical rigid ECoG electrode arrays, because they create non-conformal contacts with brain tissue resulting in high electrode/cortical tissue impedance and low-quality ECoG. One possibility, although restricted, to explore the flexibility of the SWCNT array in rats is to bend it at the scalp temporal ridge between the dorsal and lateral convexity of the brain. For this purpose, in the present study SWCNT/MD-PE arrays were implanted in rats subdurally on the dorsolateral curvilinear cortical surface. Some investigations are available with electrode arrays placed on the cortex of the lateral brain convexity in rodents using gold electrodes [14, 31] and few other studies with CNT electrode arrays placed on the cortex of the dorsal brain convexity [7, 16], but no attempts have yet been made to examine the stability and efficiency of the electrical contacts with the underlying brain tissue and the feasibility of ECoG recordings after bending and placing the array in a way that follows the curvilinear cortical surface of both the dorsal and lateral convexity of the brain.

The aims of the study were: (i) to examine the electrical functionality of SWCNT-based ECoG arrays in *in-vivo* experiments in rats; (ii) to check the flexibility of the SWCNT arrays as compared to Pt arrays of similar architecture; (iii) to compare the electrical functionality of the SWCNT and Pt electrodes in terms of electrode/cortical tissue impedance measurements *in-vivo*; (iv) to evaluate the biocompatibility of the implanted arrays in terms of histological and immunoreactive responses in the underlying cortical layers and analysis of neurological and behavioral status of rats implanted with SWCNT-based ECoG arrays; (v) to demonstrate the ability of a SWCNT-polymer based electrode to capture reliable extracellular synaptic responses in *ex-vivo* experiments using rat brain slices. Our results may serve as a background to propose the application of SWCNT-based electrode arrays in clinical practice as a part of BMI technology for neural motor prosthesis that can enable people paralyzed by disorders such as amyotrophic lateral sclerosis or ischemic stroke to achieve succesful closed loop control of movements or to control seizures in patients with medically intractable epilepsy.

2. Methods

2.1. Fabrication and characterization of ECoG devices for the in-vivo experiments

Details of the fabrication technology for the SWCNT/MD-PE devices can be found in [29]. A schematic layout of the fabrication is given in figure S1 (available online at stacks.iop.org/JNE/17/036032/mmedia) of the supplementary data. In this study we used three different types of ECoG arrays: (i) four ECoG arrays having only SWCNT tracks/electrodes (SWCNT-based ECoG array, figure 1(a)); (ii) one mixed array, having both the SWCNT and Pt tracks/electrodes (SWCNT-Pt-based ECoG array, figure 1(b)); (iii) one array with only Pt tracks/electrodes (Pt-based ECoG array with the same architecture as in (a)). We will use in the remaining text the term array (instead of grid) because the electrodes are distributed in a variable pattern along the SWCNT (or Pt) conductive tracks. The position of the electrodes in each array was tailored to be compliant to the cortical regions of interest. The conductive tracks and electrodes in all the arrays were deposited and grafted in a medium-density polyethylene (MD-PE) film substrate (weight, 0.94 g cm^{-3}, thickness 25 μm, dimensions 4 mm $\times$ 22 mm). Apertures in the film were drilled by Pulsed Laser Ablation (PLA) in micrometrically determined positions. These apertures exposed micrometric areas (diameter $\sim$50 μm) in the conductive SWCNT tracks deposited on the opposite face of the film (figure 1). The openings in the tracks served as ECoG recording sites (electrodes, probes, contacts) when positioned on the cortical surface. The polymeric film substrate served as insulating membrane between the conductive tracks and the cortex (pia mater). The SWCNT conductive tracks (0.4–0.7 mm wide) were deposited by drop casting of a suitable suspension taking care that the sensing microapertures were completely obstructed by the SWCNT track (figure 1). The center-to center track distance was 0.9 $\pm$ 0.1 mm. On observing by optical microscopy at 100x magnification, no detached material was detected in the concentrated dried solution after 5 min of sonication of the devices (at 80 kHz) in 10 cc of purified water. Platinum tracks (0.5 mm wide) were deposited by Pulsed Laser Deposition (PLD) through suitable stencils. The surface of the Pt target was locally vaporized in a plasma plume and deposited as a thin film on the sample, facing the target. The micro-drilled MD-PE film was completely protected by a metal mask except for the area to be covered by the conductive tracks (figure 1(b)). To obtain recording areas comparable to those of the SWCNT electrodes, each Pt electrode was made of a pattern of 3 $\times$ 3 microapertures (figure 1(b)), partially obstructed by the Pt deposition (<10 μm diameter). Further details on the fabrication process can be found in the supplementary data.

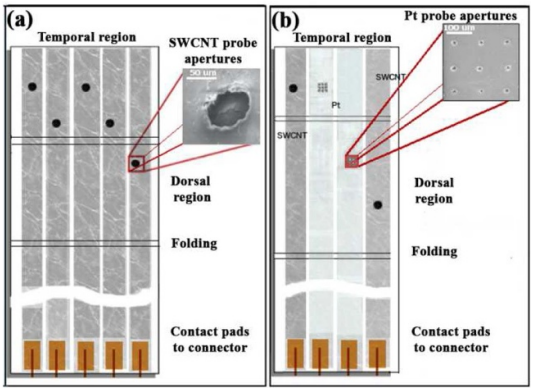

Figure 1. (a) Sketch of the SWCNT/MD-PE ECoG array, as seen from the brain side, with five SWCNT conducting tracks at the back of the transparent polymer film and the five probe sites (contacts, electrodes) exposed by the micrometric apertures (black dots and corresponding SEM image inset). The four apertures (black dots) in the SWCNT tracks (dark grey) cover the lateral brain convexity (temporal region, primary somatosensory cortex), while the single aperture below contacts the dorsal convexity, parietal association cortex. The lower folding lines correspond to the edge of the window cut in the skull, through which the remaining part of the SWCNT tracks lead to the connector outside the skull via five contact pads on which metal microwires are soldered. (b) A similar architecture for the mixed device (SWCNT-Pt-based array) is shown having two electrode sites opened in two SWCNT tracks (dark grey) and two electrode sites opened in two Pt tracks (light grey). Since the Pt vapour can not obstruct the apertures, a different design with 9 smaller holes (SEM image inset) was necessary to achieve a contacting surface of the size comparable to that of the SWCNT electrodes.

2.2. Surgery for *in-vivo* experiments on rats

The procedures used in this study were approved by the Ethics Committee of I.R.C.C.S. Neuromed and by the Italian Ministry of Health. An internal protocol for cleaning and sterilization of each device was followed before its implantation in the rat's brain, in order to eliminate as much bacterial contamination of the tissue as possible. The main steps of the surgery procedures are shown in figure 2. Each animal was anesthetized and fixed into a stereotaxic frame (World Precision Instr., FL). First, two stainless-steel screws, serving as reference (Ref) and ground (GND) electrodes, were fixed epidurally into the skull of the left hemisphere (figure 2(a)). Another 4 screws were fixed to the skull to serve for implant anchoring. The temporal muscles of the right hemisphere were cut in the lateral direction in order to have access to the lateral convexity of the brain. A cranial rectangular window (marked in figure 2(a)) was made in the right hemisphere with dimensions almost equal to those of the part of the ECoG array containing the electrodes. Then, using an optical stereomicroscope, the dura mater was carefully cut near the anterior and both lateral margins of the open bone window and retracted over the posterior bone margin in such a way that the exposed pia surface remained clean and undamaged (figure 2(b)). The device was secured to the stereotaxic holder and the ECoG array was positioned in

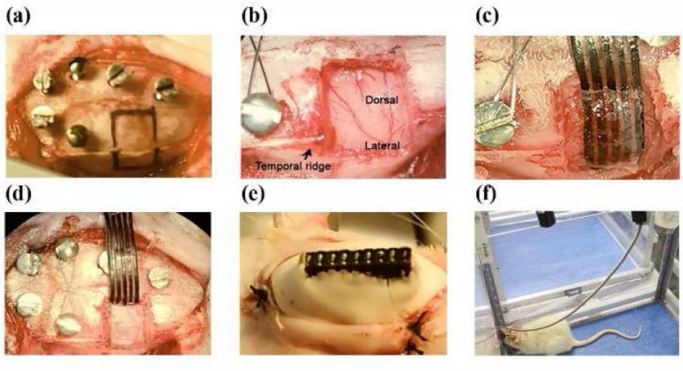

Figure 2. Surgery procedures. (a) View from above the rat's head with 6 screws fixed on the skull (4 for anchoring and two for Ref and GND). The position of the bone window is outlined with a black marker; (b) Cortical surface after removing the bone and dura mater in the window. Temporal ridge of the skull between the lateral temporal and dorsal parietal regions of the cortex is marked with an arrow; (c) The ECoG array positioned in the bone window and covered with the dura; (d) The ECoG array covered with the bone flap. The remaining part of the device (the connector and interfacing wires bent underneath) is placed on the unopen skull of the left hemisphere; (e) The rat's head with cement cup of the implant; (f) The rat in the ECoG recording box one week after the surgery.

direct contact with the cortical surface. Then the dura mater and the bone flap were repositioned over the ECoG array (figure 2(d)). The connector was finally cemented onto the skull with the help of the screws fixed to the bone (figure 2(e)).

2.3. Measurement of electrode/cortical tissue impedance *in-vivo*

In order to evaluate the performance of the electrodes in the ECoG arrays, *in-vivo* impedance measurements were performed between each electrode and the Ref electrode, immediately after the end of surgery and before each of the eight ECoG recording sessions (once a week for two months). For this purpose, an impedance meter (model EZM 4, Astro-Med, Inc. GRASS, W. Warwick RI, U.S.A) was used, which delivered 1 mA alternating current with frequency of 30 Hz to the electrodes.

2.4. *In-vivo* ECoG recording and analysis

After the surgery, a recovery period of 7 d was given to the animals before starting the ECoG recordings. Each animal was placed into a transparent box situated in an acoustically and electrically shielded room for at least 2 h before each ECoG recording for habituation to the box. The ECoG recordings were acquired using Grass-Telefactor acquisition system (Astro-Med, Inc. W. Warwick, RI, USA) with a sampling frequency of 400 Hz and 12 bit digital resolution. The ECoG array was connected to the recording system using a cable attached to a rotating system and a weighted counterbalance arm allowing unrestricted mobility of the animal in the box. The animal behavior was recorded with a video recorder simultaneously with the ECoG across 8 weeks post-implantation of the grids (once per week). The assessment of the quality of ECoG and long-term feasibility of the SWCNT arrays was made by calculating the power spectra of the ECoG using Hamming-windowed Fast Fourier Transformation (FFT) in the range of frequencies up to 200 Hz, Continuous Wavelet Transform (CWT, analytic Morse wavelet), Power Spectral Density (PSD), signal-to-noise ratio (SNR), mean power (MP), median frequency (MF_{50}), and spectral edge (SE_{95}). The ECoG records were visually inspected off-line and 4-seconds ECoG epochs were selected during passive (quiet) waking (PW) state, when the rat was in a sitting or lying down position without performing any activity. Epochs with artifacts due to grooming were discarded by inspection of the simultaneous video recordings of the rats's behavior. PSD was computed by Welsh approximation algorithm after removing slow drifts (detrending) and the mean of the signal (baseline correction). In addition, the values of the spectral power values for each of the 30 epochs were integrated for the following six frequency bands (FB): delta (0.4–4 Hz), theta (4–8 Hz), alpha (8–13 Hz), beta (13–30 Hz), gamma-1 (30–80 Hz), and gamma-2 (80–200 Hz). The power of these spectral bands was calculated and expressed as percentage of the total power. The CWT and SNR were computed by means of a custom home made script in MATLAB environment. The SNR was determined as the ratio of PSD of the signal (mean of 30 ECoG epochs of 4-s duration) to that of the noise (mean of 30 epochs of noise of 4-s duration). We performed 32 ECoG recordings of 2-hours duration (once per week) with 4 rats implanted with SWCNT-based arrays each having 5 electrodes, thus for the 8 week duration of the experiments, we had 160 channels of recorded ECoG. The noise was recorded for 5 min at the end of each ECoG recording by disconnecting the recording system from the animal's implant, thus the noise in the SNR referred to any voltage measured by the amplifier that was not representing brain activity.

2.5. Assessment of biocompatibility of chronically implanted ECoG arrays

The biocompatibility analyses included: (i) histological examination (Nissl staining); (ii) immunohistochemistry for neuronal marker NeuN, glial and microglia markers GFAP (Glial fibrillary acidic protein) and Iba1 (Ionized calcium binding adaptor molecule 1), respectively; and (iii) assessment of behavioral and neurological status of the rats and their body weight. For the histological and immunohistochemical analyses, all animals were sacrificed after the end of the experiments (two months after the implantation of the device). The devices were removed carefully, the dissected brains were fixed in the Carnoy's solution (60% ethanol, 30% chloroform and 10% glacial acetic acid), and embebbed in paraffin. Coronal sections of 10 μm thickness were sampled every 300 μm. To assess the presence of cellular damage or cortical cytoarchitecture alterations, a Nissl staining was performed on deparaffinized sections. The analysis was performed on images acquired at 5X magnification in the ipsilateral dorsal and lateral parts of the cortex below the ECoG array and symmetrically in the contralateral hemisphere. Moreover, the cortical thickness was measured on images acquired at 2.5X magnification in three different points under the ECoG array by using NIH image 1.61. As a marker of inflammatory infiltration were quantified Nissl + nuclei with a small diameter (5 μm) on acquired images at 100X magnification. For immunohistochemical analyses, deparaffinized 10 μm sections were incubated overnight at +4 °C with the following primary antibodies: mouse monoclonal anti-NeuN (1:100, Millipore, Billerica, MA, USA, codeMAB377), mouse monoclonal anti-GFAP (1:300, Sigma-Aldrich, Milan, Italy, code G3893) or rabbit polyclonal anti-Iba1 (1:200, Fujifilm Wako Pure Chemicals Corporation, Osaka, Japan, code 019–19 741). Then, the sections were incubated for 1 h at room temperature with a secondary biotinylated anti-mouse IgG (Vector Laboratories, Burlingame, CA, USA, code BA2000) or Alexa-Fluor 488 conjugated anti-rabbit IgG (Invitrogen, Milan, Italy, code: A21206). For NeuN and GFAP immunostaining, the 3,3-diaminobenzidine tetrachloride (Sigma-Aldrich) was used as chromogen substrate. For Iba1 immunostaining, before incubation with the primary antibody, the sections were treated for antigen retrieval with citrate buffer (10 mM, pH 6.0) heated in a microwave for 20 min. The percentage of neurons with a reduced or absent nuclear NeuN immunoreactivity was examined on images acquired at 100X magnification. Quantification of GFAP- and Iba1-labeled cells were performed on images acquired at 20X magnification. Cell density was determined by dividing the total number of positive cells by the area of the outlined region. All the analyses were performed for cortical tissue underneath the implanted SWCNT-based arrays (ipsilateral cortex) and symmetrical contralateral nonimplanted cortex.

The biocompatibility of any device implanted in the brain includes the preservation of normal behavioral and neurological status of the animal. In order to assess whether the animals experienced unilateral sensorimotor deficits (contralateral to the implanted hemisphere), which might happen if there was a great mechanical pressure by the implanted ECoG array on the cortical surface, a 4-score grading neurological test was applied to the rats [32]. The four scores were determined on the base of the rats neurological deficits observed, explained in the table 1(A). We assigned score of 3 to a rat with a normal neurological state, score 2 to a rat with a slight neurological deficit, score 1 to a rat with a moderate neurological deficit, and score 0 to a rat with severe neurological deficit. In addition, each animal was observed for its general behavioral status (table 1(B)). Finally, the behavior of each animal was characterized by a total score, which was the sum of the total neurological score (table 1(A)) and general behavioral score (table 1(B)). The behavioral scoring and measurement of body weight were made presurgically and once a week starting from the first week after the surgery until the end of the experiments (week 8).

2.6. Fabrication and characterization of SWCNT/polyamide composite wire probes. ex-vivo measurements

In order to probe thin and extremely delicate brain slices with no damage and high spatial precision, a thin, soft and flexible specific electrode was fabricated. A 40 mm long polyamide (PA) fishing line, 0.30 mm diameter (Caperlan Line Resist) was immersed in a SWCNT dispersion for 5 min and then heated at 110 °C. The procedure was repeated five times to obtain a homogenous layer of SWCNT on the total surface of the polyamide (PA) wire. Then the conductive SWCNT/PA wire was inserted in the signal wire of a BNC coaxial cable insulated by a heat shrinkable sheath (figure 3) and finally soldered to the connector's pin. The resistivity (measured after deposition of the SWCNT) varied in different devices, from 0.6 to 2 kOhm cm^{-1}. Local Field Potentials (LFPs) were recorded from transverse hippocampal and neocortex slices (400 μm thick) from P40–P50 Wistar rats, prepared as described elsewhere [33]. The procedure was in accordance with the regulations of the Italian Animal Welfare Act approved by the local authority veterinary service. Briefly, animals were decapitated after being anesthetized with 2-Bromo-2-Chloro-1,1,1-trifluoro-ethane. The brain was quickly removed from the skull and placed in ice-cold artificial glycerol-based cerebrospinal fluid containing (in mM) Glycerol 130, KCl 3.5, NaH2PO4 1.2, NaHCO3 25, MgCl2 1.3, CaCl2 2, glucose 10,

Table 1. Behavioral examination of rats implanted with ECoG arrays.

A. Examination of neurological deficit		
Item	Side	Grade
Rat suspended by tail:		
Flexion of forepaw and/or hindlimb	Ipsilateral	0
	Contralateral	I
Shoulder adduction	Ipsilateral	0
	Contralateral	I
Full twisting of the body	Ipsilateral	0
	Contralateral	I
Note: Latin numeral I was assigned when we observed either a flexion of contralateral forepaw/hindlimb or contralateral shoulder adduction or full twisting of the contralateral side of the body.		
Rat placed on the table:		
Asymmetry in resistance (reduced resistance toward the contralateral side)	Ipsilateral resistance < than contralateral resistance	II
Spasmodic turning of the body	Ipsilateral	0
	Contralateral	III
Consistent circling	Ipsilateral	0
	Contralateral	IV
Neurological scores: *3—normal behavior (absence of I, II, III, and IV)* *2—slight neurological deficit (presence of I or II)* *1—moderate neurological deficit (presence of I and II)* *0—severe neurological deficit (presence of I + II + III + IV)*		

B. Examination of general behavior		
Item	Behavior	Score 1—if present 0—otherwise
Passive behavior	Sleeping	1
	Standing Still	1
	Sitting still	1
Active behavior	Running	1
	Walking	1
Explorative behavior	Digging	1
	Sniffing	1
	Rearing	1
Automatic behavior	Eating	1
	Drinking	1
	Licking	1

Normal general behavioral score (table 1(B)) = 11Total score = neurological score (table 1(A)) + general behavioral score (Table 1B). The total score for normal neurological and behavioral state of rats the total score = 11 + 3 = 14

saturated with 95% O2-5% CO2 (pH 7.3–7.4). After 1 h, an individual slice was transferred to the recording chamber where it was continuously superfused with oxygenated ACSF at a rate of 2–3 ml min^{-1} at 25 °C. All drugs were purchased from Sigma or Tocris Bioscience (Bristol, UK) and freshly prepared before the experiments. Local Field potentials (LFPs) were evoked by minimal stimulation of the Schaffer collateral when recorded at CA1 stratum radiatum in hippocampus and by minimal stimulation of L4 when recorded at L5 region of neocortex. The stimulus (100 μs long in duration and amplitude in a range of 4–10 V) was used with bipolar twisted tungsten stereotrodes (2 MOhm impedance, WPI) every 30 s. In hippocampus, the following High Frequency Stimulation (HFS) protocol was applied: after 15 min of baseline (one stimulus every 30 s) recorded at CA1 stratum radiatum, 1 s burst of equally spaced pulses at 100 Hz was applied to Shaffer Collateral. LFP amplitude were followed for 1 h after the HFS.

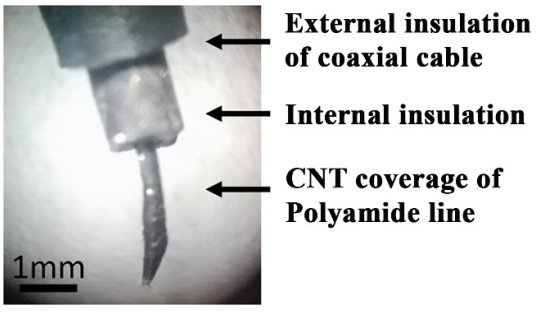

Figure 3. Optical image of SWCNT/PA composite wire for ex-vivo electrical activity recording.

2.7. Statistics

We used in this study two types of devices: 6 devices for the *in-vivo* experiments and one device for the *ex-vivo* experiments. Six rats were used for the *in-vivo* experiments, each rat was implanted with only one ECoG array. Four of the six ECoG arrays had 5 SWCNT electrodes (SWCNT-based ECoG array), one ECoG array had 2 SWCNT and 2 Pt electrodes (SWCNT-Pt-based ECoG array), and one had 3 Pt electrodes (Pt-based ECoG array). The *in-vivo* measurements of the impedances of the electrodes/cortical tissue contacts were made in all 6 rats once a week up to 2 months, starting just after the implantation of the arrays. Thus, we made for the whole experiment (total 9 weeks including the day just after the implantation) 198 measurements of the impedances with 22 SWCNT electrodes and 45 measurements with 5 Pt electrodes. For the ECoG analysis of the conformational contacts of the SWCNT electrodes on the curvilinear dorsolateral cortical surface (one electrode on the dorsal parietal cortex and one electrode on the temporal lateral cortex), we used two recordings (at week 1 and week 8) with 3 Wistar rats (3 SWCNT-based arrays) in which 30 epochs of 4-s duration for each electrode channel were chosen. Thus, we made comparison between 180 epochs in dorsal ECoG with 180 epochs in lateral ECoG. Two-way repeated measures analysis of variance (ANOVA) and Fisher LSD post-hoc test were applied for the statistics of data with the statistical package 'Statistica 7.0' (Statsoft, Inc. Tulsa, OK, USA). The behavioral and histological data were analyzed with one-way ANOVA, Fisher LSD and Dunnet or Wilcoxon matched pairs post-hoc test. The bars in the figures are mean ± standard deviation (s.d.). The differences were considered significant with minimum value of significance level $P < 0.05$.

3. Results

The following analyses were performed of: (i) electrical performance of SWCNT- and Pt-based ECoG arrays under strain; (ii) *in-vivo* electrode/cortical tissue impedance; (iii) spectral analysis of ECoG; (iv) biostability of the ECoG arrays; (v) biocompatibility of the arrays; (vi) e*x-vivo* evoked local field potentials.

3.1. Electrical performance of SWCNT- and Pt-based arrays under strain

We investigated whether Pt-based arrays could match the 3D compliance of SWCNT-based arrays. To this aim, we fabricated one Pt-based ECoG array with an architecture as close as possible to that of the SWCNT-based array and one mixed array with Pt and SWCNT electrodes (see Paragraph 2.1). We then compared their performances with that of the SWCNT-based ECoG arrays before the implantation and during *in vivo* experiments after explantation of the devices after the end of the experiments (see Paragraphs 3.2 and 3.4). The examination of the resistance versus strain for both types of materials, SWCNT and Pt, on the same polymer substrate (figure 4(a)) showed that the conductance of the SWCNT decreased regularly on stretching the conductor, although with a double slope, suggesting different regimes of conductance for strains up to 70% and more, while the Pt wire broke at very small strains (2.5%). Figure 4(b) shows an optical image of SWCNT and Pt parallel tracks under a small strain; minor stretch marks are seen as a result of strain in the SWCNT track. The less elastic Pt track, although appearing more uniform, lost its electrical conductance with a small strain, of the order of 2%. This may in principle be enough to withstand the mechanical stress caused by movements of the rat brain.

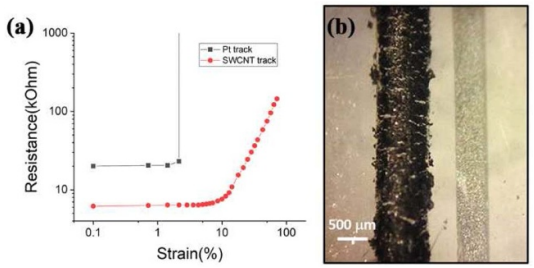

Figure 4. Characterization of resistance of SWCNT and Pt tracks to different strains. (a) Double log-plot of resistance vs strain for SWCNT and Pt tracks deposited on the MD-PE film. (b) Optical microscopic photo of parallel SWCNT (black) and Pt (grey) tracks after 5% stretching of the array.

3.2. Electrode/cortical tissue impedance

The average electrode/cortical tissue impedance of all investigated SWCNT electrodes at the day of surgery (just after implantation, at w0) did not differ substantially from that of the Pt electrodes (3.5 ± 0.7 kOhm, n = 22 electrodes in 5 arrays and 6.7 ± 3.4 kOhm, n = 5 electrodes in 2 arrays, respectively, mean ± s.d.). The first week after implantation (w1), the impedance of the SWCNT electrodes was slightly enhanced, while that of the Pt electrodes increased substantially (figure 5(a)). The average impedance of all SWCNT electrodes across the 2-months long *in-vivo* experiments was approximately 10 kOhm (n = 198 measurements) and that of the Pt electrodes was 66 kOhm (n = 45 measurements). Two-way repeated measures ANOVA on the electrode/cortical tissue impedance values showed highly significant effects ($p < 0.001$) of factors 'Type of electrodes' (SWCNT and Pt), 'Weeks' (w1, w2, w3, w4, w5, w6, w7, and w8), and their interaction. The values of the Pt electrodes were much more dispersed than those of the SWCNT electrodes (figure 5(b)).

3.3. ECoG analysis

Results obtained on the reliability and stability of the ECoG recorded by the SWCNT arrays implanted

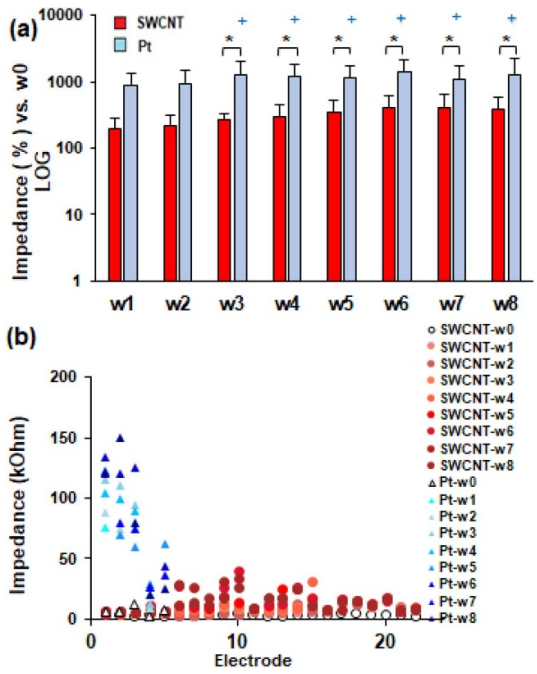

Figure 5. Analysis of the in-vivo electrode/cortical tissue impedances of SWCNT and Pt electrodes in the implanted ECoG arrays. (a) Average relative impedances during 8-weeks of experiments (percent of the values at w0—just after the implantation, logarithmic scale on y-axis) of all SWCNT electrodes (n = 22 in 5 arrays,) and Pt electrodes (n = 5 in 2 arrays) for each week from w1 to w8. *—Comparisons between impedances of SWCNT (red bars) and Pt (blue bars); +—Comparisons vs. impedance at w1. $P < 0.05$ was accepted as statistical significance in the post-hoc Fisher LSD test applied after 2-way repeated ANOVA; (b) Distribution of the impedance values (y-axis) measured at each week (from w0 to w8) for all SWCNT and Pt electrodes (x-axis). Legend on the right: white circles (SWCNT) and triangles (Pt) are for the measurements at w0. The increasing intensity of color shades are for measurements from w1 to w8 as follows: for the SWCNT electrodes (circles) from light coral to brown; for the Pt electrodes (triangles) from light blue to dark blue. Note: Some of the electrodes in each group had almost equal values of impedance at some time points and an overlap of corresponding symbols occurred.

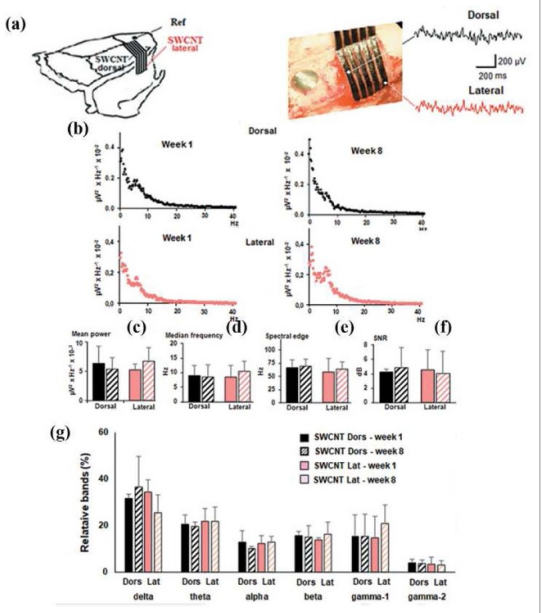

Figure 6. Comparison of characteristics of dorsal and lateral ECoG recorded by the SWCNT electrodes. (a) On the left, a scheme of the SWCNT/MD-PE array positioned subdurally on the dorso-lateral cortical surface of rats; on the right, a real photo of the ECoG array positioned on the cortex and the corresponding 1-s ECoG fragments from the dorsal and lateral cortical regions are shown; (b), (c), (d), (e), (f), and (g)—averaged values (3 arrays in 3 rats, 30 ECoG epochs of 4-s duration for each electrode, week 1 and week 8 in each rat) of PSD, Mean power, Median frequency, Spectral edge, Signal-to-noise ratio, and Relative power (% of total power) in delta, theta, alpha, beta, gamma-1, and gamma-2 frequency bands, respectively.

on the dorsal cortical surface (parietal cortex) in rats (figures 6(a) and (b)) were coherent with those obtained in our previous study [29]. The spectral parameters of the parietal dorsal ECoG (MP, MF_{50}, SE_{95}, SNR, and FB) were stable and reliable (figures 6(c)–(g) dorsal). Repeated two-way ANOVA did not show statistically relevant effects of the factor 'Week' on any of the characteristics of the ECoG recorded from the dorsal parietal cortex, which means that the ECoG was stable starting already from the first week after implantation of the ECoG array until the end of the experiments. The median frequency MF_{50} showed that 50% of the power of the dorsal parietal ECoG was below 7.6 Hz, and 50%—at higher frequencies of the spectrum. The calculated spectral edge SE_{95} revealed that 67.4 Hz was the frequency at which the power was separated into 95 and 5%. The SNR was 5 ± 2 dB (mean ± s.d.). All investigated ECoG features (PSD, MP, MF50, SE95, SNR, and FB) did not change over time ($p > 0.05$ in comparison of w1-w8).

Further, in order to ascertain that the ECoG array positioned on the dorsolateral curvilinear cortical surface made good conformal contacts of the electrodes with the cortex, we made a comparison of the electrode/cortical impedance and ECoG spectral characteristics for the primary somatosensory cortex situated in the lateral temporal region with those of the dorsal parietal cortex. The averaged impedance of the SWCNT electrodes positioned on the lateral surface (13.5 kOhm, n = 17 electrodes, 3 rats) did not differ from that of the SWCNT electrodes placed on the dorsal surface (14.0 kOhm, n = 5 electrodes, 3 rats), both measured at week 8. The two-way repeated measures ANOVA on the spectral ECoG parameters (figures 6(c)–(g)) did not show statistically significant effect of the factor 'Dorsal/Lateral'.

To further characterize the quality of the ECoG signals recorded by means of the electrodes in the SWCNT-based ECoG arrays, a recording of the ECoG during quiet (passive) waking (PW), slow wave (SWS-1 and SWS-2) and paradoxical REM sleep was made (figure 7(a)). We used validated criteria for the sleep stages identification [34]. During PW, there was a mix of low-voltage fast and slow ECoG waves. During SWS, the rats usually were lying down on the

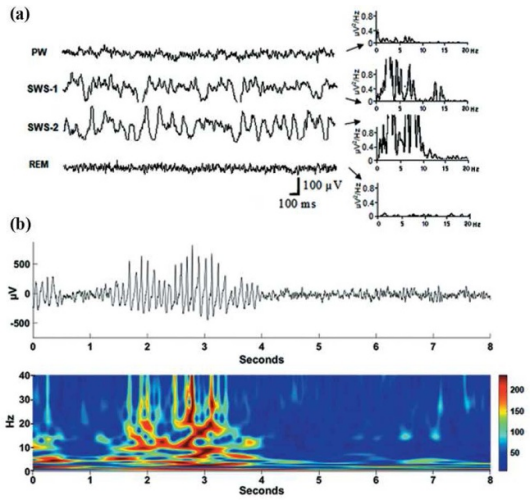

Figure 7. Examples of ECoG recorded by SWCNT-based ECoG array. (a) Representative ECoG during different vigilance states: PW, SWS-1, SWS-2, and REM. On the right, PSDs of single 4-s ECoG epochs during each vigilance state are shown. The values of PSDs during SWS were much greater than those during PW and REM; (b) ECoG recorded from the perioral primary somatosensory cortex of a WAG/Rij rat containing SWD (upper panel) and the corresponding continuous wavelet transform (lower panel).

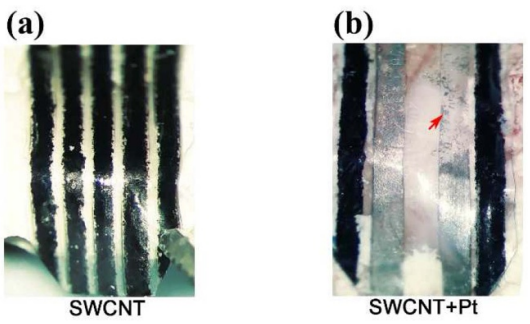

Figure 8. Optical microscopy photos of two explanted ECoG arrays. (a) ECoG array with five SWCNT tracks (black); (b) ECoG array with two SWCNT tracks (black) and two Pt tracks (grey). Regions in the Pt tracks with strong delamination of the platinum foil from the MD-PE film are shown with small red arrows.

abdomen and the cortical ECoG progressively became slower and increased in amplitude (0.4–10 Hz and 200–300 μV). Slow waves and typical sleep spindles were recorded during SWS-1, while the ECoG waves were slower and higher in amplitude during SWS-2 compared with SWS-1. During REM sleep, the ECoG waves were of low-amplitude (50–80 μV) and high-frequency (20–40 Hz). The simultaneous video-stream recording was used to check the behavior of rats as additional criteria for the waking-sleep stages identification.

Next, in order to prove that the contacts of the SWCNT electrodes with the cortical surface of the lateral convexity were suitable to record reliable ECoG, we implanted one device in a rat from the colony of adult WAG/Rij rats, which represents a validated model of absence epilepsy [35]. Well-characterized absence epilepsy-like spike-wave discharges (SWD) were recorded from the perioral cortical surface in the lateral convexity. The plot of continuous wavelet performed on a 8s ECoG epoch showed pre-SWD increase in the low frequency bands (delta, theta) and an increase in the wavelet energy at approximately 10 Hz during the SWD (figure 7(b)).

3.4. Biostability of the ECoG arrays

The ECoG arrays were explanted two months after the implantation in order to examine their biostability. Optical microscopic investigation of the explanted ECoG arrays showed that there was no damage to the material of the SWCNT tracks in any of the four SWCNT-based ECoG arrays (figure 8(a)). On the contrary, there was a severe delamination of the platinum foil from the MD-PE film in the mixed ECoG array with two SWCNT and two Pt tracks (figure 8(b)). Such Pt delamination could be due either to damages occurring during the surgery or to the lack of compliance of the Pt deposition to polymer film stretching (greater than 2% allowed by our tracks as measured in figure 4) caused by movements of the rat brain.

3.5. Biocompatibility of the ECoG arrays (histological, immunohistochemical and behavioral analyses)

The cytoarchitecture analysis of the cortical tissue showed no or very small indentation of the tissue underneath the SWCNT-based ECoG arrays. The comparison of the cortical thickness in three different portions of the cortex (dorsal, medio-lateral and ventro-lateral) revealed that the implanted array had negligible impact on the thickness of the underlying cortex (figure 9(a), right panel). Nissl stained sections (figure 9(b)) showed an intact neuropil with no evident loss of neurons underneath the ECoG array. We assessed the number of Nissl-positive nuclei with small diameter as an indiction of inflammatory infilitration, and we found no difference between the ipislateral and contralateral side (figures 9(b) and (c)). Neuronal density ($NeuN^+$ cell density) also did not change (figures 9(b1) and (c1)), suggesting the absence of neuronal death. This was also suggested by the absence of cells stained with Fluoro-Jade, which is an indicator of neurons undergoing degeneration [36]. However, we cannot exclude that implantation might have caused a mild neuronal damage because there was a trend in the percentage of $NeuN^+$ cells harboring an abnormal phenotype (figures 9(b1) and (c2)). The occurrence of neurodegeneration has been evaluated by performing a Fluoro-Jade staining of cortical tissues of implanted rats [36]. Although the difference in the density of $GFAP^+$ and $Iba1^+$ cells between the ipsilateral and contralateral sides was not statistically significant, there was a strong trend to an increase in the ipsilateral side (figures 9(b2), (b3),

(c3) and (c4)), suggesting the presence of mild reactive gliosis in the implanted cortex.

To check whether the observed neuronal damage in the cortex underlying SWCNT-based arrays could have any functional consequence, we assessed the neurological status, the behavior and body weight (figure 10). If there was severe mechanical pressure or neuronal damage in the underlying cortex caused by the implanted SWCNT-based array, an asymmetry in posture of the animal, abnormalities in muscle tone, loss of coordination, weakness, and paralysis of contralateral limbs could be expected [37]. In contrast, no behavioural abnormalities were seen. There were no seizures such as facial automatism, limb clonus, clonic jerks, or general tonic-clonic convulsions over the whole timeframe of the experiments. Before surgery, the combined score of the neurological status (table 1(A)) and behaviour (table 1(B)) was $11 + 3 = 14$ ($n = 4$ rats implanted with SWCNT-based ECoG arrays), which was indicative of a normal behavior. One week after the implantation, there was a small reduction of the score which, however, increased to 14 afterwards and retained this value until the end of the experiment (figure 10(a)). Figure 10(b) shows the body weight of rats implanted with SWCNT-based ECoG arrays. There was a decrease in the mean weight after 1 week because two animals had abnormal feeding behavior. Later, the weight recovered and increased as a function of age.

3.6. *Ex-vivo* recordings of evoked local field potentials

To assess the possibility of using SWCNT devices to record synaptic signals produced by selected neuronal populations in brain slices, an electrode specifically designed to this purpose was fabricated. With this device it was possible to record clear evoked synaptic volleys in slices from adult rat temporal cortex (figure 11(a)), which exhibited multiple waves reversibly abolished by applying tetrodotoxin (TTX, 1 μM; figures 11(b) and (c)), a selective blocker of Na^+ voltage dependent channels, which physiologically generate action potentials. Furthermore, the SWCNT-based electrode allowed the recording of evoked synaptic local field potentials in the CA1 region of adult rat hippocampus, which were clearly enhanced by high frequency stimulation in the CA3 region, as expected from previous studies (figures 11(d) and (e)) [38]. All these data show that the SWCNT-based electrode was able to record local field potentials generated by neuronal activation resulting from the stimulation of afferent fibers fibres in slices prepared from different brain regions.

4. Discussion

We have demonstrated that SWCNT/MD-PE arrays are able to record chronically reliable subdural ECoG in awake, behaving rats and that SWCNT-based electrode can detect evoked synaptic LFPs in brain slice preparations. First, we have examined in greater detail (with respect to our previous study [29]) the electrical characteristics of the SWCNT-based ECoG arrays implanted subdurally on the rat cortex in an *in-vivo* chronic setup (eight weeks). We chose to record subdural ECoG because it provides optimal signal-to-noise and finer spatial and temporal fidelity in comparison with the noninvasive standard G [2, 39].

The electrodes in the SWCNT-based ECoG arrays with diameter of approximately 50 μm showed an optimal low values of electrode/cortical tissue impedance measured *in-vivo* (mean 10.3 kOhm), much lower than the theoretically expected megaohms values of impedance for electrodes with such dimensions [40]. These relatively small values of impedance mean that the SWCNT electrodes may offer perspective for low-noise and high-quality ECoG recordings even with further miniaturization to micrometer or nanometer levels. The low noise levels of SWCNT-based electrodes in grids implanted in humans should enormously facilitate the extraction of feasible ECoG features for use in any practical neurological domain and especially for BMI application. We have also shown that the electrode/cortical tissue impedance and the computed ECoG parameters were stable over the entire time frame of the experiments (eight weeks), demonstrating the feasibility of such ECoG arrays for chronic long-term use.

The flexibility and stretchability of the composite material is of critical importance for interfacing subdural ECoG arrays with the curvilinear surface of the cerebral cortex, because the flexible substrate will decrease the mismatch between the implant and the soft brain tissue, thus reducing tissue damage and the inflammation response. Both materials incorporated in the presented devices, the conductive SWCNT and the MD-PE substrate have compliant properties to meet these requirements. Bundles made of SWCNT are extremely flexible, stretchable, and yet robust [41], while the MD-PE film substrate was chosen because ofits flexibility, plasticity, excellent chemical resistance and biocompatibility. More importantly, the composite of the polymer MD-PE and SWCNT has stretchable-viscoelastic properties, as demonstrated in our previous study [29]. The examination of the ECoG features after bending and placing the ECoG array in such a way to follow the curvilinear cortical surface of both the dorsal and lateral convexity of the brain showed that the SWCNT-based ECoG arrays were able to record feasible ECoG from both the somatosensory cortex (upper lip region situated in the lateral brain convexity) and parietal association cortex (situated in the dorsal brain convexity) with matching spectral characteristics. The occurence of similar overall ECoG

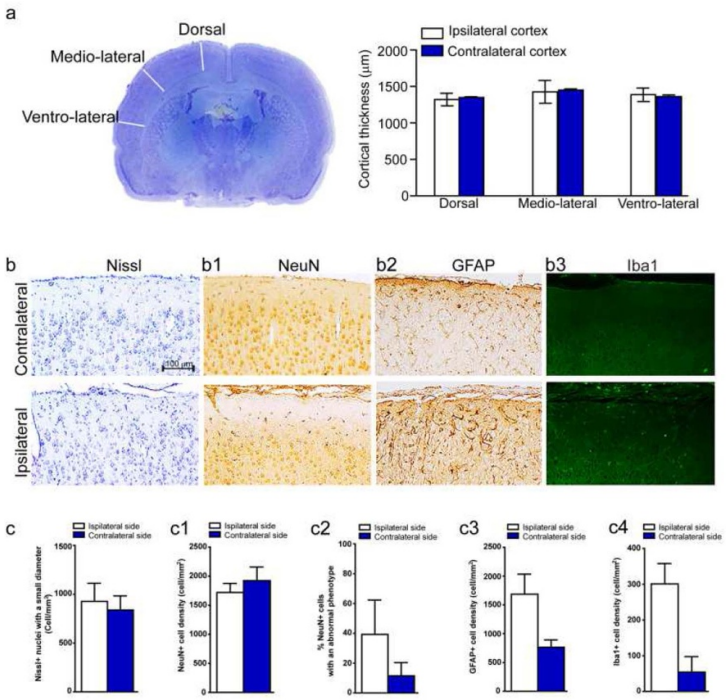

Figure 9. Histological and immunohistochemical characterization of the cortical tissue underneath the implanted ECoG arrays. (a) On the left—a representative image of a Nissl stained coronal section. On the right, analysis of the cortical thickness (μm) measured at three indicated levels. There was no statistically significant difference for the cortical thickness between the three levels or between the implanted and contralateral cortex in rats with SWCNT-based array. (b,b1,b2,b3) Nissl staining, NeuN, GFAP and Iba1 immunohistochemistry in cortical tissues of rats implanted with SWCNT-based arrays. Scale bar: 100 μm. Quantification of Nissl + nuclei with a small diameter (compatible with gliosis and inflammatory infiltration), NeuN cell density, percentage of neurons with a reduced or absent nuclear NeuN immunoreactivity (a feature of damaged neurons) and GFAP- or Iba1-immunoreactive cell density (markers of reactive gliosis or microgliosis, respectively) in the implanted cortex of rats with SWCNT- based arrays are shown in c,c1,c2,c3,c4, respectively. There is no statistically significant difference between the values of all four parameters measured in the ipsilateral and contralateral cortices. Wilcoxon matched-pairs test, $p > 0.05$, $n = 3$ rats, 3–4 cortical sections in each rat. Data are expressed as mean ± s.d.

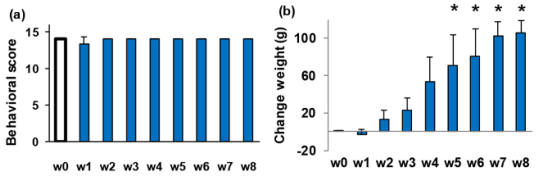

Figure 10. Characterization of the behavioural state and body weight of rats implanted with SWCNT-based ECoG arrays. (a) Assessment of global behavioural state before the surgery (at w0) and for each week from w1 to w8. (b) Changes in body weight of the same rats measured at the same time points. * One-way repeated measures ANOVA and Dunnett post-hoc test for comparisons of the weight at w1-w8 with that at w0.

patterns in both dorsal and lateral regions is consistent with the amplitude-frequency profile of EEG measured in normal subjects during quiet waking (without body movements). Such a pattern spreads along wide cortical areas and reflects diffuse excitability changes [42]. This matching may be disrupted by a somatosensory stimulation, by movements, or by a pathological process affecting these cortical areas. We took much care in our experiments to not influence the normal background conditions by using a nonpathological rat strain (a Wistar rat), to exclude any influence from the envoironment (sound isolated EEG room), and to analyse only ECoG epochs free of movement artifacts. The flexibility, stretchability and compliance of subdural ECoG arrays is very important especially for recordings in humans, because their gyrencephalic brain has an irregular topography with important cortical regions hidden inside the sulci, which are impossible to reach with the classical rigid grids. Successful attempts have been made to record ECoG by grids placed intrasulcus in monkeys [43], cats [44] and humans [45]. Although our ECoG arrays were tested on rat cortex, in which gyrification is essentially absent, this study demonstrated for the first time that the arrays can follow the curvature of the cortical surface between the dorsal and lateral convexities of the rat brain, thus preserving an excellent electrode-tissue contact. This approach could increase the possibility for closed-loop systems to target distant locations in the cerebral cortex [46]. The devices implanted into living organism must be biocompatible, that is, they must minimally disrupt the function of healthy tissues. Indeed, one of the key requirements for these devices is to ensure long-term use without triggering tissue reaction [4]. Contrary to penetrating electrodes, which disrupt brain tissue and vasculature, lead to chronic inflammatory

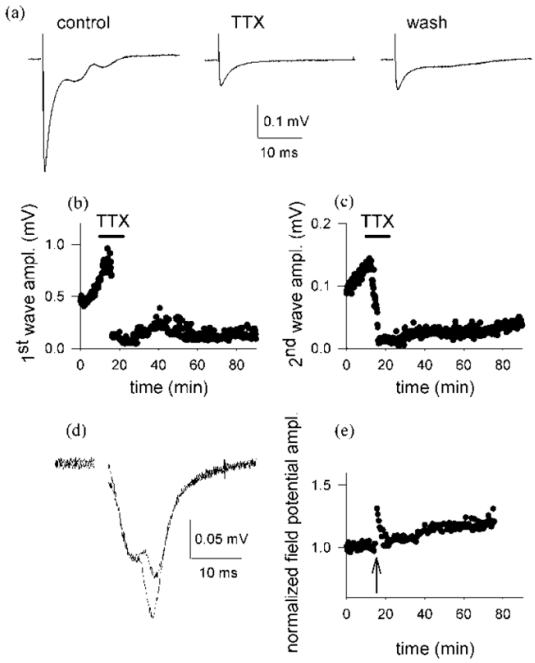

Figure 11. Evoked synaptic potentials recorded with a SWCNT-based electrode in different regions of adult rat brain slices. (a) Typical traces of evoked local field potential, recorded from the temporal cortex of an adult rat in a transversal slice, before (left), during (middle) and after the application of TTX 1 μM; (b) Time course of the amplitude of the first potential wave, same experiment as in (a). Please note the strong reduction due to TTX application, slowly reverted upon 1 h of washout; (c) Time course of the amplitude of the second potential wave, same experiments as in (a); (d) Typical superimposed traces of local field potential recorded in the CA1 hippocampal region evoked by stimulation at the Shaffer collateral, before and after high frequency stimulation; (e) Time course of the evoked local field potentials, same experiments as in (d). Please note the transient potentiation induced by the high frequency stimulation (arrow), followed by a slower amplitude increase.

response and progressive neuronal degeneration at their vicinity [47], the flat (planar) ECoG arrays avoid blood-brain barrier disruption and mechanical strain between the electrodes and soft brain tissue. Although SWCNT is the strongest known material, its bundles could potentially include graphitic debris of nanometric or even subnanometric size, which, if not surrounded by the polymer matrix, may penetrate the brain tissue. However, in contrast to the reported meningeal response after placement of metal grids [48], we did not observe any encapsulation or reduction of Nissl and NeuN positive cells in the underlying cortex. We found only a mild reactive gliosis and microgliosis (increase in the signal intensity of GFAP or Iba1 labeling astrocytes, respectively). The cytoarchitectural and histological analyses of cortical layers underneath the implanted SWCNT-based ECoG arrays did not reveal either reduction of cortex thickness or loss of neurons, as opposed to the observed great mechanical depression of a monkey brain due to the use of grid similar to those commonly used for epilepsy monitoring [49]. In rats implanted with SWCNT arrays, we did not observe in rats implanted with SWCNT arrays clinical complications like those seen in patients implanted with subdural grids [8, 9, 50].

The assessment of the neurological status and body weight of rats implanted with SWCNT-based ECoG arrays further confirmed their biocompatibility, because if there was some damage of the sensorimotor cortex caused by the implanted ECoG array, this would have caused motor deficits [37], and also a decrease in sensory thresholds, i.e. a decrease in the ability to discriminate the properties of tactile stimuli or identify objects by touch, which would decrease the ability of rats to handle the food pallets. We showed that the implanted SWCNT-based ECoG arrays did not alter the normal behavior and weight of the animal for the whole duration of the experiments.

We developed an original flexible mixed ECoG array in which two types of tracks/electrodes, SWCNT and Pt, were embedded. The comparison between their characteristics is affected by the fact that metal depositions are intrinsically unsuitable for extensible conductors. Indeed, our physical-chemical characterization of both materials showed that, while the SWCNT tracks maintained acceptable values of impedance for strains up to 70%, the Pt tracks lost their conductance at very low strains. The biostability analysis made after the ECoG arrays explant, demonstrated that, while the SWCNT tracks never lost their adhesion to the MD-PE film, a delamination of the Pt tracks from the film was observed, which shows evidence that viscoelastic surface electrodes cannot make use of Pt. In addition, the observed delamination of the Pt electrodes may cause tissue damage and aggravate inflammatory responses observed with the biocompatibility analysis. Thus, while SWCNTs are particularly suitable for stretchable

and mouldable devices, Pt thin tracks are very fragile and cannot be strained except by extremely small amounts.

In-vivo measurements of impedance of electrode-cortical interfaces showed that while the initial (first week after the implantation) impedance of the SWCNT electrodes in the implanted ECoG arrays did not change significantly from that measured just after the implantation, the impedance of the Pt electrodes raised significantly. This might be due to presence of an initial tissue response to the implanted Pt-based array. One possible explanation of the lower impedance of the SWCNT electrodes compared to the Pt electrodes is the higher effective surface of the SWCNT due to the porous nature of its bundled structure. The high surface area combined with the inherently outstanding conductivity and stability makes CNT and, in particular the SWCNT bundles, a promising active nanomaterial for highly sensitive neural interfaces [27]. The problem of the mechanical mismatch between the electrodes and the soft tissue during placement and in long- term settings is of particular importance for practice, because the rigid devices often fail due to intensive scar-tissue encapsulation induced by micro-motions between the hard materials and surrounding tissues [4, 47]. Also, the very fragile Pt tracks could easily be damaged when the ECoG array was bent and manipulated during implantation. In fact, the averaged *in-vivo* impedance of the Pt electrodes in the ECoG arrays was almost seven times greater than that of the SWCNT electrodes, that, as it is well known [51], should result in a large noise contribution producing unacceptable SNR and noisy ECoG.

Even though chronic subdural implantation of grids has been made previously in animals (mainly using metal electrodes) [7, 14–16], almost nothing is known about the quality of the ECoG and most importantly whether the characteristics change over time. Pre-surgical ECoG monitoring of patients with drug-resistant epilepsy lasts normally less than 28 d (usually one week) because of the risk of complications [8, 9, 52]. Our 2-month study in rats revealed that the relative power of high-frequency ECoG bands (alpha, beta, and gamma-1) captured by means of the SWCNT-based electrode arrays was stable and even increased from week 1 to week 8, which might be explained by the optimal and stable contact of the SWCNT electrodes with the cortical surface. Quantitative analysis of the spectral content of the ECoG showed that the SWCNT electrodes had high F_{95}, which demonstrated that they were able to catch high frequencies components of the ECoG. High frequencies are of specific interest for control of movements by BMI, because they carry substantial information about movements [53]. One possible explanation of the low impedance, the high SNR, and the high quality of the ECoG signal captured by the SWCNT electrodes is the high effective surface of the SWCNT due to the porous nature of its bundled structure. The high surface area combined with the inherently outstanding conductivity and stability makes CNT and, in particular the SWCNT bundles, a promising active nanomaterial for highly sensitive neural interfaces [27]. Moreover, we have demonstrated the reliability of as-prepared SWCNT ECoG arrays to record well-differentiated ECoG across wake-sleep cycle in a healthy Wistar rat and also to capture well-characterized pathological absence epilepsy-like spike-wave discharges from the primary somatosensory cortex (perioral region) of a WAG/Rij rat. Although SWDs are generalized over the cortex, the cortical source driving these discharges is shown to be situated in the primary sensory cortex, which is a part of the cortico-thalamo-cortical network underlying absence seizures [54]. The time-frequency characteristics of the SWDs recorded by our SWCNT-based ECoG arrays were coherent with those recorded by conventional metal electrodes [35, 55].

Finally, we demonstrated for the first time that the SWCNT can be used as a material to create flexible electrodes for *ex-vivo* recording of synaptic LFPs in brain slices. The *ex-vivo* experiments served only to further demonstrate that the SWCNT is a suitable material for capturing of neuronal electrical activity and to support the *in-vivo* results obtained with the flat subdural ECoG arrays. In fact, our SWCNT-based electrode was able to record evoked synaptic potentials both from slices prepared from the temporal cortex and hippocampus of adult rats. In addition, we showed that it was possible to resolve well-described and expected pharmacologically or electrically-induced signal modulation in both regions. In particular, we demonstrated that a selective blocker of voltage-activated Na^+ channels reversibly abolished evoked signals in the temporal cortex [56], while high frequency stimulation induced long-term potentiation (LTP) of excitatory synaptivc transmission in the hippocampus [57]. These results show that our SWCNT-based electrode is adequate to acquire reliable synaptic information from selected neuronal subpopulations present in brain slices.

5. Conclusions

To the best of our knowledge this is the first study that demonstrates, in both *in vivo* and *ex-vivo* experiments, the electrical and biocompatibility properties of chronic neural interfacing of SWCNT-based ECoG arrays in the rat cerebral cortex. The fabricated SWCNT-based ECoG arrays met the specific requirements to be used as a chronically implantable part of BMIs [2]. The SWCNT-based ECoG arrays had appropriate mechanical properties such as softness, flexibility and surface compliance, relatively low electrode-tissue impedance, optimal SNR, and high

biocompatibility to supply high-quality and stable ECoGs in a chronic setup. As a future perspective, our results lay the graundwork for the use of SWCNT-based ECoG arrays for the development of new cortical implants for opened and closed-loop BMI systems with various clinical applications, such as absence epilepsy and motor disturbances after stroke. The study has some limitations that will be addressed in our future studies, such as the small sample size, the relatively short time frame of the experiments, and the limited properties of the used EEG hardware.

Author contributions

LP conceived the study. LP and SM conceptualized and designed the experiments, performed the ECoG and impedance recordings and analyzed the data, wrote and reviewed the manuscript. PM, LF, AP, and RS fabricated the ECoG arrays and SWCNT-based ex-vivo electrode and performed the electrical characterization of the devices before their implantation. LF and AP made the corresponding figures for the fabrication process and characterization. LP performed the wavelet analysis of the absence epilepsy-like ECoG seizures. SM designed the concept and supervised the surgeries, carried out the statistical analyses and made the figures of ECoG, impedance and behavioral data. FM performed the surgeries, explantation of the devices, histological examination and made the corresponding figures. AG managed the animals, sterilized the devices, assisted in the ECoG and impedance recordings and performed behavior measurements. SF and KM performed and analyzed the ex-vivo recordings, and wrote the corresponding part in the manuscript. CB and DB performed and analyzed the immunohistochemistry examination and wrote the appropriate portion of the content. FM, PM, LF, AP, and RS contributed to drafting the manuscript. FN and FF contributed to the revision of the final version of the manuscript. All authors declare that they have no competing financial interests.

ORCID iD

Luigi Pavone https://orcid.org/0000-0002-0454-9784

References

[1] Leuthardt E C, Schalk G, Wolpaw J R, Ojemann J G and Moran D W 2004 A brain-computer interface using electrographic signals in humans *J. Neural. Eng.* **1** 63–71
[2] Schalk G and Leuthardt E C 2011 Brain-computer interfaces using electrocorticographic signals *IEEE Rev. Biomed. Eng.* **4** 140–54
[3] Fukushima M, Chao Z C and Fujii N 2015 Studying brain functions with mesoscopic measurements: advances in electrocorticography for non-human primates *Curr. Opin. Neurobiol.* **32** 124–31
[4] Kotov N A *et al* 2009 Nanomaterials for neural interfaces *Adv. Mater.* **21** 3970–4004
[5] Poole-Warren L, Lovell N, Baek S and Green E 2010 Development of bioactive conducting polymers for neural interfaces *Expert Rev. Med. Dev.* **7** 35–49
[6] Geddes L A and Roeder R 2003 Criteria for the selection of materials for implanted electrodes *Ann. Biomed. Eng.* **31** 879–90
[7] Henle C, Raab M, Cordeiro J G, Dookstam S, Schulze-Bonhage A, Stieglitz T and Rickert J 2011 First long term in vivo study on subdurally implanted micro-ECoG electrodes, manufactured with a novel laser technology *Biomed.Microdev.* **13** 59–68
[8] Önal Ç, Otsubo H, Araki T, Chitoku S, Ochi A, Weiss S, Logan W, Elliott I, Snead O and Rutka J T 2003 Complications of invasive subdural grid monitoring in children with epilepsy *J. Neurosurgery* **98** 1017–26
[9] Fong J S, Alexopoulos A V, Bingaman W E, Gonzalez-Martinez J and Prayson R A 2012 Pathologic findings associated with invasive EEG monitoring for medically intractable epilepsy *Am. J. Clin. Pathol.* **138** 506–10
[10] Wu C, Evans J J, Skidmore C, Sperling M R and Sharan A D 2013 Impedance variations over time for a closed-loop neurostimulation device: early experience with chronically implanted electrodes *Neuromodulation* **16** 46–50
[11] Jeong J W, Shin G, Park S I I, Yu K J, Xu L and Rogers J A 2014 Soft materials in neuroengineering for hard problems in neuroscience *Neuron* **86** 175–86
[12] Scaini D and Ballerini L 2018 Nanomaterials at the neural interface *Curr. Opinion Neurobiol.* **50** 50–55
[13] Hong G and Lieber C M 2019 Novel electrode technologies for neural recordings *Nat. Rev. Neurosci.* **20** 330–45
[14] Hollenberg B A, Richards C D, Richards R, Bahr D F and Rector D M 2006 A MEMS fabricated flexible electrode array for recording surface field potentials *J. Neurosci. Meth.* **153** 147–53
[15] Hosp J A, Molina-Luna K, Hertler B, Atiemo C O, Stett A and Luft A R 2008 Thin-film epidural microelectrode arrays for somatosensory and motor cortex mapping in rat *J. Neurosci. Meth.* **172** 255–62
[16] Khodagholy D, Doublet T, Gurfinkel M, Quilichini P, Ismalova E, Leleux P, Herve T, Sanaur S, Bernard C and Malliaras G 2011 Highly conformable conducting polymer electrodes for in vivo recordings *Adv. Mater.* **23** H268–272
[17] Sauter-Starace F, Bibari O, Berger F, Caillat P and Benabid A L 2009 ECoG recordings of a non-human primate using carbon nanotubes electrodes on a flexible polyimide implant *Proc. of the 4th Int. IEEE/EMBS Conf. on Neural Engineering* pp 112–5
[18] Chen Y C *et al* 2011 An active, flexible carbon nanotube microelectrode array for recording electrocorticograms *J. Neural Eng.* **8** 034001
[19] Zhang H, Patel P R, Xie Z, Swanson S D, Wang X and Kotov N A 2013 Tissue-compliant neural implants from microfabricated carbon nanotube multilayer composite *ACSNano* **7** 7619–29
[20] Khudhair D, Nahavandi S, Bhatt A, Garmestani H and Bhatti A 2017 Microelectrode arrays: architecture, challenges and engineering solutions *Emerging Trends in Neuro Engineering and Neural Computation* (Berlin: Springer) pp 41–59
[21] Voge C M and Stegemamm J P 2011 Carbon nanotubes in neural interfacing applications *J. Neural Eng.* **8** 011001
[22] Wang K, Fishman H A, Dai H and Harris J S 2006 Neural stimulation with a carbon nanotube microelectrode array *Nano Lett.* **6** 2043–8
[23] Malarkey E B and Parpura V 2007 Applications of carbon nanotubes in neurobiology *Neurodegenerative Dis.* **4** 292–9
[24] Gabay T, Ben-David M, Kalifa I, Sorkin R, Abrams Z R, Ben-Jacob E and Hanein Y 2007 Electro-chemical and biological properties of carbon nanotube based multi-electrode arrays *Nanotechnology* **18** 035201
[25] Shein M, Greenbaum A, Gabay T, Sorkin R, David-Pur M, Ben-Jacob E and Hanein Y 2009 Engineered neuronal circuits shaped and interfaced with carbon nanotube microelectrode arrays *Biomed. Microdev.* **11** 495–501

[26] Odom T W, Huang J-L, Kim P and Lieber C M 1998 Atomic structure and electronic properties of single-walled carbon nanotubes *Nature* **391** 62–4
[27] Bareket-Keren L and Hanein Y 2013 Carbon nanotube-based multi electrode arrays for neuronal interfacing: progress and prospects *Front. Neural Circuits* **6** 122
[28] Kim T, Cho M and Yu K J 2018 Flexible and stretchable bio-integrated electronics based on carbon nanotube and graphene *Materials* **11** 1163
[29] Morales P, Moyanova S, Pavone L, Fazi L, Mirabile M D, Rapone B, Gaglione A and Senesi R 2018 Self-grafting carbon nanotubes on polymers for stretchable electronics *Europ. Phys. J. Plus* **113** 214
[30] Ribas G C 2010 The cerebral sulci and gyri *Neurosurg. Focus* **28** E2
[31] Konerding W S, Froriep U P, Kal A and Baumhoff P 2018 New thin-film surface electrode array enables brain mapping with high spatial acuity in rodents *Sci. Rep.* **8** 3825
[32] Moyanova S G, Kortenska L V, Mitreva R G, Pashova V D, Ngomba R T and Nicoletti F 2007 Multimodal assessment of neuroprotection applied to the use of MK-801 in the endothelin-1 model of transient focal brain ischemia *Brain Res.* **1153** 58–67
[33] Martinello K, Sciaccaluga M, Morace R, Mascia A, Arcella A, Esposito V and Fucile S 2018 Loss of constitutive functional γ- aminobutyric acid type A-B receptor crosstalk in layer 5 pyramidal neurons of human epileptic temporal cortex *Epilepsia* **59** 449–59
[34] Gottesmann C 1992 Detecton of seven sleep-waking stages in the rat *Neurosci. Biobehav. Rev.* **16** 31–38
[35] Van Luijtelaar G and Coenen A M L 1986 Two types of electrocortical paroxysms in an inbred strain of rats *Neurosci. Lett.* **70** 393–7
[36] Schmued L C, Albertson C and Slikker W Jr. 1997 Fluoro -Jade: a novel fluorochrome for the sensitive and reliable histochemical localization of neuronal degeneration *Brain Res.* **1997** 37–46
[37] Schallert T, Fleming S M, Leasure J L, Tillerson J L and Bland S T 2000 CNS plasticity and assessment of forelimb sensorimotor outcome in unilateral rat models of stroke, cortical ablation, parkinsonism and spinal cord injury *Neuropharmacol.* **39** 777–87
[38] Taube J S and Schwartzkroin P A 1998 Mechanisms of long-term potentiation: EPSP/spike dissociation, intradendritic recordings, and glutamate sensitivity *J.Neurosci.* **8** 1632–44
[39] Petroff O A, Spencer D D, Goncharova I, I and Zaveri H P 2016 A comparison of the power spectral density of scalp EEG and subjacent electrocorticograms *Clin. Neurophysiol.* **127** 1108–12
[40] Robinson D A 1968 The electrical properties of metal microelectrodes *Proc. IEEE* **56** 1065–71
[41] Kulik A J, Kis A, Lukic B, Lee K and Forró L 2007 Mechanical properties of carbon nanotubes *Fundamentals of Friction and Wear. NanoScience and Technology* ed E Gnecco and E Meyer (Berlin: Springer) pp 583–600
[42] Steriade M, Gloor P, Llinás R R, Lopes da Silva F H and Mesulam -M-M 1990 Basic mechanisms of cerebral rhythmic activities *Electroenceph. Clin. Neurophysiol.* **76** 481–508
[43] Fukushima M, Saunders R C, Mullarkey M, Doyle A M, Mishkin M and Fujii N 2014 An electrocorticographic electrode array for simultaneous recording from medial, lateral, and intrasulcal surface of the cortex in macaque monkeys *J.Neurosci. Meth.* **233** 155–65
[44] Viventi J, *et al* 2011 Flexible, foldable, actively multiplexed, high-density electrode array for mapping brain activity in vivo *Nat.Neurosci.* **14** 1599–605
[45] Yanagisawa T, Hirata M, Saitoh Y, Kato A, Shibuva D, Kamitani Y and Yoshimine T 2009 Neural decoding using gyral and intrasulcal electrocorticograms *Neuroimage* **45** 1099–106
[46] Guggenmos D J, Azin M, Barbay S, Mahnken J D, Dunham C, Mohseni P and Nudo R J 2013 Restoration of function after brain damage using a neural prosthesis *PNAS* **110** 21177–82
[47] Fattahi P, Yang G, Kin G and Abidian M R 2014 A Review of organic and inorganic biomaterials for neural interfaces *Adv. Mater.* **26** 1846–85
[48] Schendel A A *et al* 2014 The effect of micro-ECoG substrate footprint on the meningeal tissue response *J. Neural Eng.* **11** 046011
[49] Degenhart A D *et al* 2016 Histological evaluation of a chronically-implanted electrocorticographic electrode grid in a non-human primate *J Neural Eng.* **13** 046019
[50] Lee W S, Lee J K, Lee S A, Kang J K and Ko T S 2000 Complications and results of subdural grid electrode implantation in epilepsy surgery *Surg Neurol.* **54** 346–51
[51] Cogan S F 2008 Neural stimulation and recording electrodes *Ann. Rev. Biomed. Eng.* **10** 275–309
[52] Nair D R, Burgess R, McIntyre C C and Luders H 2008 Chronic subdural electrodes in the management of epilepsy *Clin.Neurophysiol.* **119** 11–28
[53] Schalk G, Miller K J, Anderson N R, Wilson J A, Smyth M D, Ojemann J G, Moran D W, Wolpaw J R and Leuthardt E C 2008 Two-dimensional movement control using electrocorticographic signals in humans *J. Neural Eng.* **5** 75–84
[54] Meeren H K M, Pijn J P M, van Luijtelaar E L J M, Coenen A M L and Lopes da Silva F H 2002 Cortical focus drives widespread corticothalamic networks during spontaneous absence seizures in rats *J. Neurosci.* **22** 1480–95
[55] Midzianovskaia I S, Kuznetsova G D, Coenen A M L, Spiridonov A M and van Luijtelaar E L J M 2011 Electrophysiological and pharmacological characteristics of two types of spike-wave discharges in WAG/Rij rats *Brain Res.* **911** 62–70
[56] Melnikova D I, Khotimchenko Y S and Magarlamov T Y 2018 Addressing the issue of tetrodotoxintargeting *Mar Drugs.* **16** E352
[57] Herring B E and Nicoll R A 2016 Long-term potentiation: from CaMKII to AMPA receptor trafficking *Annu. Rev. Physiol.* **78** 351–65